

Numerical modeling of Asian dust emission and transport with adjoint inversion using LIDAR network observations

K. Yumimoto¹, I. Uno², N. Sugimoto³, A. Shimizu³, Z. Liu⁴, and D. M. Winker⁵

¹Department of Earth System Science and Technology, Kyushu University, Fukuoka, Japan

²Research Institute for Applied Mechanics, Kyushu University, Fukuoka, Japan

³National Institute for Environmental Study, Tsukuba, Japan

⁴National Institute of Aerospace, Hampton, Virginia, USA

⁵NASA Langley Research Center, Hampton, Virginia, USA

Received: 12 October 2007 – Accepted: 2 November 2007 – Published: 14 November 2007

Correspondence to: K. Yumimoto (yumimoto@riam.kyushu-u.ac.jp)

Numerical modeling of Asian dust with adjoint inversion

K. Yumimoto et al.

Title Page

Abstract

Introduction

Conclusions

References

Tables

Figures

◀

▶

◀

▶

Back

Close

Full Screen / Esc

Printer-friendly Version

Interactive Discussion

Abstract

A four-dimensional variational (4D-Var) data assimilation system for a regional dust model (RAMS/CFORS-4DVAR; RC4) is applied to a heavy dust event which occurred between 20 March and 4 April 2007 over eastern Asia. The vertical profiles of the dust extinction coefficients derived from NIES LIDAR observation network are directly assimilated. We conduct two experiments to evaluate impacts of selections of observation sites: Experiment A uses five Japanese observation sites located only downwind of dust source regions; the other Experiment B uses these sites together with two other sites near source regions (China and Korea). Validations using various observation data (e.g., PM_{10} concentration, MODIS AOT, OMI Aerosol Index, and the dust extinction coefficient derived by space-based LIDAR NASA/CALIPSO) are demonstrated. The modeled dust extinction coefficients are improved considerably through the assimilation. Assimilation results of Experiment A are consistent with those of Experiment B, indicating that observations of Experiment A can capture the dust event correctly and include sufficient information for dust emission inversion. Time series of dust AOT calculated by modeled and LIDAR dust extinction coefficients show good agreement. At Seoul, Matsue, and Toyama, assimilation reduces the root mean square errors of dust AOT by 31–32%. Vertical profiles of the dust layer observed by CALIPSO are also compared with assimilation results. The dense dust layer was trapped between $\theta=280\text{--}300\text{ K}$ and elevated higher toward the north; the model reproduces those characteristics well. The modeled dust AOT along the orbit paths agrees well with the CALIPSO dust AOT, OMI AI, and the coarse mode AOT retrieved from MODIS; especially the modeled dust AOT and the MODIS coarse mode AOT are consistent quantitatively. Assimilation results increase dust emissions over the Gobi Desert and Mongolia considerably; especially between 29 and 30 March, emission flux is increased by about 2–3 times. The heavy dust event is caused by the heavy dust uplift flux over the Gobi Desert and Mongolia during those days. We obtain the total optimized dust emissions of 57.9 Tg (Experiment A; 57.8% larger than before assimilation) and 56.3 Tg (Experi-

ACPD

7, 15955–15987, 2007

Numerical modeling of Asian dust with adjoind inversion

K. Yumimoto et al.

Title Page

Abstract

Introduction

Conclusions

References

Tables

Figures

◀

▶

◀

▶

Back

Close

Full Screen / Esc

Printer-friendly Version

Interactive Discussion

EGU

ment B; 53.4% larger).

1 Introduction

Over eastern Asia, soil dust aerosols dominate aerosol loading. They have important effects on the atmospheric environment and climate in the springtime (e.g., Overpeck et al., 1996 and Sokolik and Toon, 1996). Numerical simulations are powerful tools to elucidate dust emission, transportation and deposition. Numerical dust models (e.g., Gong et al., 2003; Liu et al., 2003; Shao et al., 2003; Uno et al., 2004; Tanaka and Chiba, 2005) have been developed for predictions and hindcast analyses. They have provided valuable information related to characteristics of Asian dust phenomena. However, proper estimation of dust emissions is quite difficult because of their large dependence upon various parameters (e.g., soil texture, soil wetness, land-use data, and surface wind speed). Results of the recent dust model inter-comparison project (DMIP) (Uno et al., 2006) show that simulated amounts of dust emission fluxes among eight dust models differed sometimes by a factor of ten. The wide scattering of dust emissions reflects differences in dust emission schemes, surface boundary data, and atmospheric models within the models. Such uncertainty of estimation of dust emission fluxes strongly influences the model output.

Four-dimensional variational (4D-Var) data assimilation based on the adjoint model provides insights into various aspects of numerical models (e.g., initial conditions, boundary conditions, and emissions); it has been used for meteorological and oceanographic modeling (e.g., Benjamin et al., 2004; Awaji et al., 2003). As for Chemical Transport Model (CTMs), Elbern et al. (1997) and Elbern and Schmidt (1999, 2001) applied 4D-Var data assimilation to their CTM (European Air pollution Dispersion model, EURAD), and obtained valuable results related to data assimilation of ozone observations over the European region. Müller and Stavrakou (2005) and Stavrakou and Müller (2006) presented estimates of CO and NO_x emissions using the IMAGE 4D-Var system with satellite data. Hakami et al. (2005) performed an inversion estimate of

Numerical modeling of Asian dust with adjoint inversion

K. Yumimoto et al.

Title Page

Abstract

Introduction

Conclusions

References

Tables

Figures

◀

▶

◀

▶

Back

Close

Full Screen / Esc

Printer-friendly Version

Interactive Discussion

black-carbon emissions over eastern Asia with the adjoint of the STEM (Sulfur Transport Eulerian Model). Yumimoto and Uno (2006) applied 4D-Var to a regional CTM and estimated CO emissions over eastern Asia. Chai et al. (2006, 2007) developed a STEM 4D-Var System and assimilated a comprehensive observation data set during International Consortium for Atmospheric Research on Transport and Transformation (ICARTT) experiments. Henze et al. (2007) developed the adjoint of GEOS-Chem and validated its feasibility. However, compared to meteorological and oceanographic models, applications of 4D-Var for CTMs remain limited.

For assimilation of dust transport, Niu et al. (2007) developed a dust forecasting system using a three-dimensional variational method (3D-Var). They improved dust concentrations with column observation data observed by FY-2C satellite (Hu et al., 2007); however, unlike 4D-Var, 3D-Var can not adjust the source (i.e. dust emission) and can not use observation data of different observation times simultaneously. Yumimoto et al. (2007) developed 4D-Var data assimilation system of the RAMS/CFORS dust model and, using NIES LIDAR observations, estimated dust emissions of a heavy dust event observed on 30 April 2005.

For the present study, we applied RAMS/CFORS-4DVAR (RC4; Yumimoto et al., 2007) to assimilation of the transport and emission of mineral dust using NIES LIDAR network observation data, targeting a dense dust event observed over eastern Asia during late March and early April 2007. We conducted two experiments to evaluate effects of a selection of observation sites on the assimilation results. One experiment used observation sites located downwind of dust source regions. The other used these sites together with sites near source regions. The assimilation results were validated using various observation data. Surface PM_{10} concentration, dust extinction coefficient retrieved from Cloud-Aerosol LIDAR with Orthogonal Polarization (CALIOP) onboard Cloud-Aerosol LIDAR and Infrared Pathfinder Satellite Observations (CALIPSO), MODerate resolution Imaging Spectroradiometer (MODIS; aboard NASA's TERRA and AQUA satellites) AOT, and Aura Ozone Monitoring Instrument; Aerosol Index (OMI AI) were used for validation. This paper is structured as follows. Section 2 describes the

**Numerical modeling
of Asian dust with
adjoint inversion**K. Yumimoto et al.

[Title Page](#)[Abstract](#)[Introduction](#)[Conclusions](#)[References](#)[Tables](#)[Figures](#)[◀](#)[▶](#)[◀](#)[▶](#)[Back](#)[Close](#)[Full Screen / Esc](#)[Printer-friendly Version](#)[Interactive Discussion](#)

RC4 data assimilation system. Section 3 describes the model setup and observation data used in the assimilation. In Sect. 4, we show the assimilation results and their validations. Finally, conclusions are summarized in Sect. 5.

2 Methods

5 The RAMS/CFORS-4DVAR (RC4; Yumimoto et al., 2007) consists of a regional dust transport model (RAMS/CFORS; Uno et al., 2003), its adjoint model, and an optimization process. In fact, RAMS/CFORS is built on a mesoscale meteorological model, the Regional Atmospheric Modeling System (RAMS, ver. 4.3; Pielke et al., 1992), using its optional scalar transport system and embedding dust emission, gravitational settling, and dry/wet deposition scheme. Thereby, all meteorological fields from RAMS
10 are used directly for tracer advections and diffusions.

The discrete equation for the gas/aerosol tracers used in RAMS/CFORS is

$$Q(t_{i+1}) = MQ(t_i) + E dt = \{I + (M_{\text{adv}} + M_{\text{diff}} + M_{\text{reac}})dt\} Q(t_i) + E dt, \quad (1)$$

15 where Q is the dust concentration, M is the model operator, and in which M_{adv} , M_{diff} , and M_{reac} respectively represent advection, diffusion, and reaction (including gravitational settling, chemical reaction and conversion, and dry/wet deposition) operators. In addition, E denotes the emission of the species, t is the time step, and I is a unit matrix.

In the 4D-Var system, the optimal solution is obtained by minimizing a cost (objective) function:

$$20 J(C) = \frac{1}{2}(C - C_b)^T B^{-1}(C - C_b) + \frac{1}{2} \sum_{i=1}^n (H_i C - y(t_i))^T R^{-1}(H_i C - y(t_i)), \quad (2)$$

where C is designated as the control parameter, which is optimized in the assimilation process. We can set initial conditions and/or emissions, etc. as a control parameter. Also in that equation, y denotes observation, H represents the forward model operator and the transform operator from the model space into the observation vector, and B

Numerical modeling of Asian dust with adjoint inversion

K. Yumimoto et al.

Title Page

Abstract

Introduction

Conclusions

References

Tables

Figures

◀

▶

◀

▶

Back

Close

Full Screen / Esc

Printer-friendly Version

Interactive Discussion

and R respectively denote the background error covariance and the observation error covariance. The first term on the right-hand side of Eq. (2) represents a departure of the assimilated value C from the first-guess value C_b , weighted by B . The second term represents discrepancies between simulated and observed values weighted by R .

Gradients of the cost function (Eq. 2) with respect to a set of the control parameters ($\nabla_C J$) are necessary to minimize the function. In a 4D-Var system, the adjoint model is used to calculate them. An adjoint of Eq. (1) is derived as follows.

$$\begin{aligned} \lambda(t_i) &= M^T \lambda(t_{i+1}) + \partial J / \partial (H_i C) \\ &= \left\{ \mathbf{I} + (M_{\text{advc}}^T + M_{\text{diff}}^T + M_{\text{reac}}^T) dt \right\} \lambda(t_{i+1}) + \partial J / \partial (H_i C) \end{aligned} \quad (3)$$

Therein, λ represents adjoint variables. Also, M_{advc}^T , M_{diff}^T , and M_{reac}^T respectively represent adjoint operators of M_{advc} , M_{diff} , and M_{reac} . In addition, $\partial J / \partial (H_i C)$, which shows the discrepancy between simulated and measured values (i.e. residual); it drives the adjoint model as a forcing term. The adjoint model is integrated backward in time, and propagates the residual as adjoint variables (also called an influence function), which means that the adjoint model is also useful to perform sensitivity analyses (e.g. Martien et al., 2006).

In RC4, an iterative optimization routine, which applies Quasi-Newton L-BFGS (Liu and Nocedal, 1989), is used for minimization of the cost function. That optimization routine requires several integrations of both forward and adjoint models before a convergence criterion is satisfied. Meteorological fields are generated in advance by RAMS. They drive the forward and backward models in an off-line manner to reduce those computational loads. Consequently, in the current version of RC4, the meteorological fields (e.g., temperature and humidity) have no feedback of the tracer field, and were not assimilated. The convergence criterion used in this study is that the norm of the gradient of the cost function is reduced by 1/1000 with respect to the initial one.

Strong surface winds uplift mineral aerosols into the atmosphere. The current RC4 calculates the total dust uplift flux based on Uno et al. (2003, 2004), which uses a fourth

Numerical modeling of Asian dust with adjoint inversion

K. Yumimoto et al.

Title Page

Abstract

Introduction

Conclusions

References

Tables

Figures

◀

▶

◀

▶

Back

Close

Full Screen / Esc

Printer-friendly Version

Interactive Discussion

power-law function of surface friction velocity u_* , as

$$F_k = \varepsilon_{ij} C_{ij} f_k u_*^3 (u_* - u_{*,th}), \quad (4)$$

where ε represents the control parameter for optimization of dust emissions at each grid set equal to unity for the first guess (before assimilation), and C is the dimensional constant depending on surface information (e.g. soil wetness), suffix of ij denotes each grid point. In addition, u_* and $u_{*,th}$ respectively denote surface friction velocity and threshold friction velocity. The RC4 models 12 bin dust particles (radius 0.1–20 μm); k denotes each bin number. In this study, the cost function (Eq. 2) is redefined as

$$J(\varepsilon) = \frac{1}{2} (\varepsilon - \varepsilon_b)^T B^{-1} (\varepsilon - \varepsilon_b) + \frac{1}{2} \sum_{i=1}^n (H_i \varepsilon - y(t_i))^T R^{-1} (H_i \varepsilon - y(t_i)) + \frac{\gamma}{2} \|\Delta(\varepsilon - 1)\|^2. \quad (5)$$

The third term is a smoothing term to avoid unrealistic horizontal jumps of the control parameters (Carmichael et al., 2007). For our study, ε is defined as the daily constant at each model grid. To reduce the uncertainty noise of ε , the daily dust uplift fluxes are optimized. In this version of RC4, negative values of the control parameters are replaced with zeros in the last iteration.

3 Experiment setup and observations

Based on dust extinction coefficients measured using the NIES LIDAR observation network, RC4 is applied for assimilation of dust transport and inversion of dust emissions over eastern Asia. Figure 1a shows the simulation area, which is centered at 37.5° N, 115° E on a rotated polar stereographic system. The horizontal grids comprise 180×100 grids with 40 km resolution. The vertical grids comprise 40 grid points extending from the surface to 23 km with 40 stretching grid layers (140 m at the surface to 650 m at the top) in terrain-following coordinates. Meteorological boundary conditions to RAMS meteorological integration are taken from NCEP/NCAR reanalysis data

Numerical modeling of Asian dust with adjoint inversion

K. Yumimoto et al.

Title Page

Abstract

Introduction

Conclusions

References

Tables

Figures

◀

▶

◀

▶

Back

Close

Full Screen / Esc

Printer-friendly Version

Interactive Discussion

with 2.5°×2.5° resolution and a 6 h interval. For this study, the simulation is performed during 20 March–4 April 2007 with zero initial dust concentration.

At 14 locations, NIES LIDARs (Sugimoto et al., 2006; <http://www-lidar.nies.go.jp/>) are operating continuously (see Fig. 1a), measuring vertical profiles of dust outflows over eastern Asia with high spatial and temporal resolution. Their vertical and temporal resolutions are, respectively, 30 m and 15 min. The extinction coefficient is derived based on the backward Fernald's method (Fernald, 1984) by setting a boundary condition at 6 km. We used a non-zero boundary value when the retrieved aerosol profile was negative (Shimizu et al., 2004), and 50 sr as the LIDAR ratio (S1) (Liu et al., 2002). Contributions of mineral dust to the extinction coefficients were estimated using the particle depolarization ratio (Shimizu et al., 2004).

In this study, the vertical profiles of the dust extinction coefficients derived from LIDAR observation are assimilated directly. They are used to evaluate the cost function (Eq. 3). Modeled dust extinction coefficients are calculated based on Takemura et al. (2000) at every model time step. We performed two assimilation experiments to evaluate impacts on the assimilation results of the choice of observation sites. Experiment A assimilates five LIDAR sites over the Japanese Archipelago, which are located downstream of the dust source regions. Experiment B assimilates those five sites and another two sites, including both sites at downstream and near the dust source region. Consequently, Experiment A consists of Hedo-Okinawa, Nagasaki, Matsue, Toyama, and Tsukuba. Experiment B uses data of the five sites of Experiment A, with Beijing and Seoul data added (Table 1). Observation sites of each set are represented by bold circles in Fig. 1a (red circles represent observation sites used in both Experiment A and Experiment B; green circles represent sites added to Experiment B). The LIDAR data are interpolated vertically to the RC4 vertical resolution. Then 1-h averaged LIDAR dust extinction coefficients are used for data assimilation with a 3-h interval. For both observation groups, the dust extinction coefficients measured from 29 March to 4 April 2007 from surface to 4000 m height were assimilated. In this work, surface observations (e.g. PM₁₀ observations) and satellite retrievals (e.g., OMI AI, CALIPSO LIDAR

Numerical modeling of Asian dust with adjoint inversion

K. Yumimoto et al.

Title Page

Abstract

Introduction

Conclusions

References

Tables

Figures

◀

▶

◀

▶

Back

Close

Full Screen / Esc

Printer-friendly Version

Interactive Discussion

data, and MODIS aerosol optical thickness) were used only for validation: those data were not applied to data assimilation. The current RC4 can assimilate these observation results. Introduction of these data will be the next step of our application in future studies.

5 An accurate estimate of the background error (B) of the dust emission flux is important for adequate data assimilation. The dust uplift flux depends on numerous parameters (e.g., soil texture, soil wetness, land-use data, and surface wind speed). In addition, dust emissions over the inland desert region have been measured sparsely. These facts render the estimation of background error (B) of dust emission extremely
10 difficult. Uno et al. (2006) suggest that dust emission fluxes over eastern Asia differ immensely among the DMIP 8 models. The dust emission fluxes were 27–336 Tg with mean of 120 Tg for period A (March 2002), and 18–103 Tg with mean of 36.3 Tg for period B (April 2002), reflecting various differences among the models (e.g., dust emission scheme, surface boundary data, and meteorological fields). The maximum
15 of the dust emission flux of DMIP is sometimes about 600–1200% of the minimum. In this study, the background error covariance (B) for the dust emission is assumed as diagonal, with assigned uncertainty of 500% to the dust emission flux as the background error. Measurements near the source region and a detailed evaluation of the background error will help to improve the model prediction and its assimilation.

20 The observation error covariance (R) is assumed as diagonal. Sugimoto et al. (2002) estimated the error introduced by the assumption of LIDAR ratio (S_1). The extinction coefficient using $S_1=50$ sr was increased by 16% compared to that using $S_1=40$ sr, and decreased by 11% compared to that using $S_1=60$ sr at 1 km altitude. Here, the measurement error is chosen as follows (Elbern et al., 2007):

$$25 \quad B = \text{Max}(E_{\text{abs}}, Y \times E_{\text{rel}}), \quad (6)$$

where E_{abs} represents a minimal absolute error set as 0.05 km^{-1} ; E_{rel} represents a relative error rate assigned 10%.

**Numerical modeling
of Asian dust with
adjoint inversion**K. Yumimoto et al.

Title Page

Abstract

Introduction

Conclusions

References

Tables

Figures

◀

▶

◀

▶

Back

Close

Full Screen / Esc

Printer-friendly Version

Interactive Discussion

4 Results and discussion

4.1 Assimilation results

Figure 2 shows horizontal distributions of modeled AOT and the OMI AI. In the left column, colored and pink contours respectively denote assimilated AOT and OMI AI. In the right column, color represents model dust AOT without assimilation. Symbol \$ shows the dust report from the WMO SYNOP surface weather. In fact, OMI AI is also sensitive to non-dust aerosols; high AI levels observed over southern Asia are attributed to aerosols originating from biomass burning (e.g. black carbon). For 1 April, OMI AI is not available.

High-density dust, emitted over an extended desert region over north-central China and Mongolia by strong surface winds caused by a low-pressure area located at north-east Mongolia on 30 March, was transported to the east with a low-pressure system and its accompanying cold front. It reached northeast China on 31 March, extending from the East China Sea to the Sea of Japan on 1 April. It covered the Japanese Archipelago on 2 April. The modeled AOT coincides well with OMI AI and SYNOP dust reports. Generally, the modeled AOT is increased by assimilation. The assimilation results reproduce dense dust loadings centered near 105° E and 40° N on 30 March and covering Japan on 1 April, which was not reproducible using the simple CFORS model.

Figure 3 shows comparisons of observed and modeled dust extinction coefficients at Seoul, Matsue, and Tsukuba. The first and second rows respectively show observations and model results without assimilation. Blacked-out areas in observations show rain or clouds. Contour lines represent the potential temperature by RAMS. A heavy dust event occurs from 31 March to 1 April at Seoul (dust extinction coefficients exceed 2 km^{-1}), and from 1 April to 2 April at Matsue and Tsukuba. The dense dust layers are captured $\theta=285\text{--}295$ K. The potential temperature within a specific air mass can be considered to be preserved. Therefore, dust layers observed at each site are presumed to be transported from the same source region. Other observation sites

Numerical modeling of Asian dust with adjoind inversion

K. Yumimoto et al.

Title Page

Abstract

Introduction

Conclusions

References

Tables

Figures

◀

▶

◀

▶

Back

Close

Full Screen / Esc

Printer-friendly Version

Interactive Discussion

over Japan measure a similar dense dust layer, which arrived between 1 and 2 April with a dense dust extinction coefficient level ($<1 \text{ km}^{-1}$). Model results without assimilation represent the onset and overall behavior of the dust layer, but the dust extinction coefficients are underpredicted considerably during the heavy dust event.

5 The lower two rows in Fig. 3 show assimilation results. The third row shows the results of Experiment A; the fourth row shows results of Experiment B. The assimilation results compensate model dust extinction coefficients considerably and bring modeled concentrations closer to observed ones. At the Tsukuba observation site, two dust peaks observed on 1 and 2 April are reproduced and emphasized by the assimilation. The structures and onset timings of the dust layers are not modified dramatically. For that reason, the forward model itself precisely represents dust emission timings and source regions; thus, the assimilation might not adjust those considerably, but it improves the emission intensity.

15 At Seoul (Fig. 3a), dense dust layers are observed on 31 March and 1 April. The model reproduces the dust layers, including upper dense dust between 2000–3500 m on 1 April. The LIDAR observations above 2000 m between 31 March and early 1 April at Seoul are not undefined because the dust layer centered at 1000 m height was so dense that the LIDAR signal was unable to penetrate into the upper layer, which indicates that a dust loading observed at 2000–3500 m height on 1 April is continuous (not separated) with the dense dust layer on 31 March, like the modeled dust layer.

20 At the Matsue observation site (Fig. 3b), the model captures the dense dust loading that occurred between 31 March and 2 April; considerable improvements of the model dust extinction coefficients are apparent during the dense dust loading through assimilation. However, the assimilation results were incapable of reproducing an elevated dust layer on later 30 March at 3000–4000 m altitude (a similar dust layer is observed at Nagasaki; not shown). The HYSPLIT trajectory model (Draxler and Hess, 1998; <http://www.arl.noaa.gov/ready/hysplit4.html>) suggests that the air masses corresponding to the dust layers originated above the Taklimakan Desert region (not shown). That region, located in western China, is surrounded by high mountains: the Tian Shan

Numerical modeling of Asian dust with adjoint inversion

K. Yumimoto et al.

Title Page

Abstract

Introduction

Conclusions

References

Tables

Figures

◀

▶

◀

▶

Back

Close

Full Screen / Esc

Printer-friendly Version

Interactive Discussion

Mountains, Pamir Plateau, Tibetan Plateau, and Kunlun Mountains. Because of its complicated and sharp terrain, it is difficult to reproduce detailed meteorological fields (especially, wind speed and direction, and the boundary layer height; Uno et al., 2005). The resolution of the current RC4 (40 km) might not be sufficient to reproduce the dust emission and uplifting of the dust particles caused by the topography conditions (i.e., surface winds, updraft along the sharp terrain, and convection). The difficulty of meteorological simulation prevented assimilation from modifying the dust emission over this region because the adjoint model cannot propagate the required dust emission information (i.e. the residual) to the control parameter ε in Eq. (5) backward in time. Improvement of RAMS horizontal resolution might improve the assimilation performance.

Little difference is apparent between results of Experiment A and Experiment B. The Seoul observation site data are not used in Experiment A. Nevertheless, the Experiment A assimilation results improve the model dust extinction coefficient considerably, but dramatic improvement is not obtained from Experiment B. Observation sites in Experiment A are distributed widely over Japan along the meridian, which is crossed to the main dust outflow direction. This fact indicates that the observation data of Experiment A captured the dust event characteristics extensively and adequately, and increased the assimilation performance. Small differences between Experiment A and Experiment B results also indicate that the assimilated emission by Experiment A is consistent with LIDAR-observed results at Seoul and Beijing. The assimilated emissions are discussed in Sect. 4.4. Results of Experiment B are presented as our “assimilation results” in the following sections.

Figure 4 shows time series data of dust aerosol optical thickness (AOT) at LIDAR observation sites. The dust AOT is calculated through vertical integration of the dust extinction coefficient from the surface to 6000 m altitude. Circles denote the 1-h-average of dust AOT calculated using LIDAR observations; gray bars denote ranges between the minimum and maximum of LIDAR dust AOT. Red lines are assimilated dust AOTs and blue lines are those without the assimilation. Solid lines denote model dust AOTs, which take missing LIDAR points into account. Blue and orange box bars denote

**Numerical modeling
of Asian dust with
adjoint inversion**K. Yumimoto et al.

[Title Page](#)[Abstract](#)[Introduction](#)[Conclusions](#)[References](#)[Tables](#)[Figures](#)[⏪](#)[⏩](#)[◀](#)[▶](#)[Back](#)[Close](#)[Full Screen / Esc](#)[Printer-friendly Version](#)[Interactive Discussion](#)

ranges between the total AOT (box top) and coarse mode AOT (box bottom), as measured using the MODIS, which were derived from the aerosol optical depth and the aerosol optical depth ratio small provided by the Level-3 MODIS Atmosphere Daily Global Product (Remer et al., 2005). Blue bars show data observed using the onboard TERRA satellite; orange ones show data observed using the onboard AQUA satellite. It is important to mention here that the MODIS coarse mode AOT is also sensitive to non-dust aerosols (e.g. sea salt).

On 31 March, a dense dust loading was observed at Seoul. This dust loading is presumed to have reached the Beijing site on 30 March; however, weather conditions obscured the observation data. Over the Japanese islands, the dust layer was first observed at Matsue and Toyama on later 31 March, captured at Nagasaki and Tsukuba on 1 April, finally reaching Hedo-Okinawa on 2 April. The MODIS observations also measured heavy dust loading at each observation site. The model reproduced those onsets of the dust loading well.

The assimilation results improve the modeled dust AOT and agree quite well with LIDAR dust AOT. Time variations between LIDAR AOT and MODIS AOT show good agreement; the assimilation results also capture these variations well. The assimilated dust AOT is increased by 2–2.5 times compared to that before the assimilation during the dust event, which hit Beijing on 30 March, Seoul between 31 March and 1 April, and Japanese sites between 1 and 2 April.

At the Beijing observation site, because of clouds and rain that continued from 29 March to early 31 March, the LIDAR measured few vertical profiles of the dense dust layer. Between 25 March and 28 March, the simulated dust AOT was still underestimated compared to the LIDAR dust AOT. These high LIDAR dust AOT levels might reflect local dust storms and local air pollution, which were unable to reach Seoul and Japanese sites. Assimilations including observation data measured during that period might improve such differences. On 31 March, Nagasaki and Matsue LIDAR observed a dense dust, which the model was unable to reproduce. As described previously, these elevated dust layers might have originated from the Taklimakan Desert region.

Numerical modeling of Asian dust with adjoind inversion

K. Yumimoto et al.

Title Page

Abstract

Introduction

Conclusions

References

Tables

Figures

◀

▶

◀

▶

Back

Close

Full Screen / Esc

Printer-friendly Version

Interactive Discussion

Table 1 lists the root mean square (RMS) error and mean values of modeled and LIDAR dust AOT from 25 March to 4 April. Data assimilation improved the RMS errors and the biases between observed and modeled mean values. At Seoul, Toyama, and Matsue, the RMS errors are reduced by 31–32%. Experiment A shows significant improvement of the RMS error and the mean value of Seoul. At Beijing, Tsukuba, and Nagasaki, the mean AOT values are brought much closer to observed ones; however, the RMS errors are not improved in spite of the assimilation. At Beijing, local dust storms between 25 and 29 March and little data during the heavy dust event might engender that result. At Nagasaki, dust loading from the Taklimakan Desert observed on 31 March might result in the lesser improvement of the RMS error. At the Tsukuba site, the observation data of the heavy dust event are less than those at other observation sites because of upper clouds and rain (see Fig. 2c), which might explain the degradation of the RMS error.

4.2 Surface measurements

Validation of the assimilation results by observations not used for the assimilation is crucially important. Figure 5 shows comparisons of time series of surface PM_{10} at Rishiri, Banryu, Sado, and Hedo-Okinawa (shown as blue triangles in Fig. 1a). Hourly PM_{10} and $PM_{2.5}$ (at Rishiri only) observations are provided by Japan Acid Deposition Survey (JADS) of the Ministry of Environment, Japan. Dashed lines denote total dust concentrations; solid lines denote dust PM_{10} concentrations calculated for the smaller eight bins, with 0.13, 0.21, 0.33, 0.52, 0.82, 1.27, 2.01, and $3.19 \mu m$ effective radius.

The heavy dust layer was measured on later 31 March at Banryu and Sado, then reached Hedo-Okinawa and Rishiri. At Rishiri, the peak concentration of the dust layer is much smaller (about $40 \mu g/m^3$) than at the other sites (about $300\text{--}800 \mu g/m^3$) because the dust layer is elevated toward the north, as shown in the following Sect. 4.4. Two peaks of concentrations are visible at Banryu and Sado, which are also observed at the Tsukuba LIDAR site (see Fig. 3c). The model reproduces these peaks.

Considerable improvements are apparent in PM_{10} peak concentrations despite of

Numerical modeling of Asian dust with adjoint inversion

K. Yumimoto et al.

Title Page

Abstract

Introduction

Conclusions

References

Tables

Figures

◀

▶

◀

▶

Back

Close

Full Screen / Esc

Printer-friendly Version

Interactive Discussion

the assimilation using only LIDAR observations. The modeled peak concentrations are doubled or tripled by the assimilation, and show good agreement with observations. At Hedo-Okinawa, the assimilation results induce the onset time of model PM₁₀ peak to come 3 h earlier and bring closer to the observed onset time. In contrast, the assimilated PM₁₀ slightly overestimates the observed one at Rishiri. In this study, Experiment A and Experiment B did not include the LIDAR observation site located in the north region (i.e. Sapporo; see Fig. 1). Because of rain and clouds, the Sapporo LIDAR obtained only a little observation data during the dust event. Further improvements, especially over the north region, can be expected if such measurements are used for assimilation.

Table 1 also shows the RMS errors and mean values of PM₁₀ concentrations. With the exception of Sado, modeled mean concentrations are brought closer to observed ones by the assimilation. However, the assimilation degrades the RMS errors. The model results were insufficient to reproduce observed sharp peaks, especially at the end of the dust event. Experiment B presents better RMS errors, than those achieved through Experiment A because of the lesser emission amount (Sect. 4.4).

4.3 Space-based LIDAR

CALIOP onboard CALIPSO (Winker et al., 2007) is a space-based backscatter lidar launched on 28 April 2006. CALIOP is an active instrument in space that is currently providing continuous global measurements of aerosol and cloud vertical distributions. CALIOP data products are therefore an ideal data source for validating the vertical structure of the assimilated dust event. In this section, we make comparison of the assimilation results with the CALIOP products to examine our assimilation system.

CALIOP provides profiles of the total attenuated backscatter coefficient at 532 nm and 1064 nm, and the depolarization ratio at 532 nm in the Level 1B data products at horizontal resolution 333 m. Both vertical and horizontal resolutions vary for different altitude ranges due to the onboard average to reduce the data volume to be down-linked. The CALIOP Level 2 data processing finds features (cloud, aerosol, surface,

Numerical modeling of Asian dust with adjoint inversion

K. Yumimoto et al.

Title Page

Abstract

Introduction

Conclusions

References

Tables

Figures

◀

▶

◀

▶

Back

Close

Full Screen / Esc

Printer-friendly Version

Interactive Discussion

and etc.) in a lidar profile and makes classification of the features. Currently released in the Level 2 layer products are the layer averaged attenuated optical properties along with cloud-aerosol discrimination (CAD) results. The CAD score is computed based on the cloud and aerosol probability density functions (PDFs) and is used as an indicator for discrimination between clouds and aerosols for the CALIOP layer (Liu et al., 2004). It ranges between -100 and 100 ; positive values denote clouds, whereas negative values denote aerosols. The absolute value of the CAD score signifies a confidence level for the classification. Detailed descriptions can be found in the CALIPSO web page (<http://www-calipso.larc.nasa.gov/>) and references there in.

Because the extinction retrieval is not released in the current Level 2 data products, we retrieved dust extinction coefficients from the CALIOP LEVEL 1B data by the same method as that used for NIES LIDAR described earlier. The forward inversion is started from 14 km height down to ground surface with $S_1=30$ sr. In this study, the dust extinction coefficients derived from the CALIOP measurements are averaged to the horizontal resolution of Level 2 (5 km).

Figure 6 shows four CALIPSO observation paths, the modeled dust AOT, surface wind (first row), and vertical profiles of the dust extinction coefficients observed by CALIPSO (third row), as well as assimilated profiles (second row) interpolated along the orbit path. In that figure, L represents a low pressure area and red broken lines represent a cold front. The assimilated profiles are also overlaid into the third row by broken lines. The CAD scores are also shown in Fig. 6 (fourth row).

Each CALIPSO path overpasses near the center of the dense dust layer with a low pressure area; its cold front is as shown in the first row of Fig. 6. The dense dust layer emitted from north-central China and the Mongolia region moved eastward and reached the Sea of Japan on 1 April. On paths A, B, and C, the model results (second row of Fig. 6) show that the dust layer is elevated to the north along the isentropic surface of $\theta=290$ – 300 K as it travels eastward. In addition, CALIPSO (third row of Fig. 6) captures that elevated dust layer and agrees with the model results well. On path D (Fig. 6d), CALIPSO observed the dust layer over the Yellow Sea; the model also

Numerical modeling of Asian dust with adjoint inversion

K. Yumimoto et al.

Title Page

Abstract

Introduction

Conclusions

References

Tables

Figures

◀

▶

◀

▶

Back

Close

Full Screen / Esc

Printer-friendly Version

Interactive Discussion

captured the dust layer.

The CAD scores (the fourth row of Fig. 6) assess the CALIOP layers, of which dust extinction coefficients are high, as vague (near zero values). For dense dust layers, because of their relatively high backscatter coefficient and color ratio (similar to those for optically thin clouds), they generally falls in the overlap/vague region of the aerosol and cloud PDFs and the magnitude of CAD scores for this type aerosol is generally small near zero. This can be demonstrated by the dust layers (greenish colored in the CAD scores) between 38° N–46° N on path A, 34° N–42° N on path B, and 38° N–43° N on path C in the fourth row of Fig. 6. In this case, the misclassifications can happen. Liu et al. (2004) suggested that misclassification can also happen when the aerosol layer is contaminated by embedded or vertically adjacent clouds. In Fig. 2 and the first row of Fig. 6, we show that the dust plume was following the low-pressure and its accompanying cold front; CALIOP observed the area adjacent to them on path B (Fig. 6b), and close behind of them on path A (Fig. 6a) and path C (Fig. 6c). Heavy dust loading (AOT>2) lies adjacent to the cold front and co-exists with the ice-cloud, which even complicates the dust classification. The cloud and aerosol discrimination results currently released in the Level 2 layer products are beta version which are early release products for users to gain familiarity with data formats and parameters. This data product needs to be validated and the CAD algorithm is being refined for future data releases.

The fifth row in Fig. 6 presents a comparison of the modeled dust AOT, CALIPSO dust AOT, OMI AI, and MODIS coarse mode AOT interpolated along each orbit path. The modeled and CALIPSO dust AOT are calculated through vertical integration of the dust extinction coefficient from the surface to 14 km. The modeled and MODIS AOTs correspond to the left axis, CALIPSO AOT corresponds to the right inside axis, and OMI AI corresponds to the right axis. On 1 April, OMI AI was unavailable. Satellite observations are available once a day: MODIS TERRA overpasses at 10:30 LT (about 02:00 UTC over eastern Asia), MODIS AQUA crosses at 13:30 LT (about 05:00 UTC over eastern Asia), and OMI overpasses at 13:45 LT (about 05:00 UTC over eastern

Numerical modeling of Asian dust with adjoint inversion

K. Yumimoto et al.

Title Page

Abstract

Introduction

Conclusions

References

Tables

Figures

◀

▶

◀

▶

Back

Close

Full Screen / Esc

Printer-friendly Version

Interactive Discussion

Asia).

In general, the modeled AOT and observations shows good agreement, capturing the latitude at which AOTs have high values. Both MODIS TERRA and AQUA coarse mode AOT, and modeled dust AOT are quantitatively consistent (e.g., on paths B and C). Some dips are apparent on observations. For example, in path A, there are two peaks produced by a dip around 40° N, which are not found in model results, in CALIPSO dust AOT and OMI AI. This is caused by a cloud at 10 km height (see fourth row). Similar observation dips are visible around 39° N and 44° N–48° N on path B, and around 40° N and 43° N on path C. On paths B and D (Figs. 6b and d), which crossed over the Yellow Sea and near industrial regions of east China, satellite observations measure high AOT and AI (e.g., MODIS and OMI observations around lower latitudes on path B, MODIS TERRA observations on path D). These high values might be partly affected by pollution from the industrial region over east China.

Compared to modeled and MODIS coarse mode AOT, CALIPSO dust AOT gives a smaller AOT level. On paths A, B, and C, the upper dense dust layers (AOT>2) hampered penetrations of CALIPSO LIDAR signals into the lower layers, thereby engendering underestimation of CALIPSO dust AOT. For another reason, the assigned S1 value (for this study, we used S1=30) might partly affect the underestimation.

4.4 Dust emission

Figure 1 shows assimilated dust emission intensities from 20 March to 3 April. Figure 1b and c respectively depict increments obtained using results of assimilation for Experiment A and Experiment B. Both results increase dust emissions over the Gobi Desert and Mongolia; especially around the border between China and Mongolia. Distributions of increments of dust emission fluxes by Experiment A and Experiment B are very similar, but some differences exist. These differences might reflect more detailed dust storms observed at Beijing and Seoul, which were not observed over Japan: for example, a dust storm observed at Beijing on 3 April (see Fig. 4a). Meanwhile, their close similarity indicates that the assimilation results of Experiment A are

Numerical modeling of Asian dust with adjoint inversion

K. Yumimoto et al.

Title Page

Abstract

Introduction

Conclusions

References

Tables

Figures

◀

▶

◀

▶

Back

Close

Full Screen / Esc

Printer-friendly Version

Interactive Discussion

consistent with observations made at Beijing and Seoul; furthermore, an assimilation using Experiment A observations can obtain appropriate assimilation results for severe dust storms. As described before, the NIES LIDAR observation network, which is distributed widely over the Japanese Archipelago, enables Experiment A to capture the overall behavior of the dust event. Additionally, observations near the dust storm regions (e.g., Beijing, Seoul, and other new LIDAR sites) can include more detailed dust storms in assimilations, and might become crucial for real-time forecasting with a 4D-Var assimilation system.

Figure 7 shows the daily variation of dust fluxes as well as the averaged wind speed, u_* and $u_{*,th}$ in the dust source region (see Fig. 1a). Between 29 and 30 March, the assimilation increases the dust flux significantly. On 29 and 30 March, the model simulated high wind speeds and $u_{*,th}$. The strong northwest wind blew over the north-central China and Mongolia region and lifted up large amounts of dust particles into the atmosphere. On those days, the assimilation increases dust emission flux by 2–3 times, indicating that the heavy dust storm is caused by this strong surface wind over those regions on 29 and 30 March. We obtain the total optimized dust emissions of 57.9 Tg (Experiment A: 57.8% larger than without the assimilation) and 56.3 Tg (Experiment B: 53.4% larger than without the assimilation) during the assimilation window. Both results are quite consistent.

Most grids in which dust fluxes are increased considerably by the assimilation are designated as having a Loamy Sand soil texture (not shown). In the current RC4, the initial dust-size distribution of dust uplift flux is the same in all dust emission regions. The assimilation results might reflect this poor information about the dust-size distribution. Meanwhile, the control parameter ε Eq. (3) cannot reflect observation data in the dust-size distribution and $u_{*,th}$ in this study. As a future task, optimization of the dust-size distribution at each model grid might be required; however, few observations that can enable measurement of size distributions are available. Expansion of such observations is both important and necessary.

Numerical modeling of Asian dust with adjoint inversion

K. Yumimoto et al.

Title Page

Abstract

Introduction

Conclusions

References

Tables

Figures

◀

▶

◀

▶

Back

Close

Full Screen / Esc

Printer-friendly Version

Interactive Discussion

5 Concluding remarks

The 4D-Var data assimilation system for the regional dust model was applied to the dust event that occurred over eastern Asia between 20 March and 4 April 2007. The vertical profile of the dust extinction coefficients derived from LIDAR observations were assimilated directly. We performed two assimilation experiments to evaluate the impact of observation site selections on assimilation results: Experiment A used five observation sites distributed only throughout Japan (downstream of the dust source region); Experiment B used those five observation sites and two other sites nearer the dust source region (Beijing and Seoul). The assimilation results were validated using various observation data: MODIS coarse mode AOT, CALIPSO dust extinction coefficient, OMI AI, the WMO SYNOP weather report, and surface PM₁₀ concentrations. Results can be summarized as follows:

1. Dense dust loading originated from a desert region extended over north-central China and Mongolia by a low pressure system and its cold front on 30 March. It reached the East China Sea and the Sea of Japan on 1 April, and covered the Japanese Archipelago on 2 April. The modeled AOT coincides well with these dust onsets and OMI AI. The assimilation increases the modeled AOT and reproduces the dense dust loading, which was not captured before the assimilation.
2. The modeled dust extinction coefficients are improved considerably and come to resemble LIDAR dust extinction coefficients through the assimilations. The assimilation results of Experiment A are consistent with those of Experiment B. This fact indicates that observations of Experiment A can capture the dust layer comprehensively and adequately.
3. Time series of dust AOT by the model and LIDAR show good agreement. The modeled AOT can also capture MODIS coarse mode AOT variations. Assimilation results increase modeled dust AOT and improve peak dust AOT levels markedly. At Seoul, Toyama, and Matsue, the RMS errors of dust AOT are reduced by 31–

Numerical modeling of Asian dust with adjoint inversion

K. Yumimoto et al.

Title Page

Abstract

Introduction

Conclusions

References

Tables

Figures

◀

▶

◀

▶

Back

Close

Full Screen / Esc

Printer-friendly Version

Interactive Discussion

**Numerical modeling
of Asian dust with
adjoint inversion**

K. Yumimoto et al.

Title Page

Abstract

Introduction

Conclusions

References

Tables

Figures

◀

▶

◀

▶

Back

Close

Full Screen / Esc

Printer-friendly Version

Interactive Discussion

32%. Experiment A also showed improved RMS errors and mean AOT values at Seoul (not included in Experiment A).

4. Surface PM₁₀ concentrations from Japan Acid Deposition Survey (JADS) are used for independent validation of the assimilation results. The model can generally capture variations of observations and reproduce unique characteristics of two peak PM₁₀ concentrations measured at Banryu and Sado. The assimilation results double or triple the modeled peak concentrations during the heavy dust event and show good agreement with observations.
5. The assimilation results are compared with dust extinction coefficients retrieved by CALIPSO (a satellite-borne LIDAR). The model can reproduce observed dust layer characteristics, which are captured between $\theta=290\text{--}300\text{ K}$ and elevated higher toward the north, quite well. The modeled dust AOT along the orbit paths agree well with the CALIPSO dust AOT, OMI AI, and MODIS coarse mode AOT; particularly, the modeled dust AOT and the MODIS coarse mode AOT are quantitatively consistent. However, the CALIPSO dust AOT is smaller than either the modeled or MODIS coarse mode AOT. CALIPSO signal was unable to penetrate to lower layers because of dense upper dust layers ($\text{AOT}>2$), which might cause that underestimation.
6. Assimilation results show considerably increased dust emissions over the Gobi Desert and Mongolia; especially between 29 and 30 March, dust emission flux must increase by 2–3 times. Dense dust events are caused by the heavy dust uplift flux over the Gobi Desert and Mongolia during those days. We obtained total optimized dust emissions of 57.9 Tg (Experiment A, 57.8% larger than before assimilation) and 56.3 Tg (Experiment B, 53.4% larger than before assimilation) during the assimilation window. Distributions of increments of dust fluxes by Experiment A and Experiment B are similar. This similarity indicates that the assimilation results of Experiment A are consistent with observations at Beijing and

Seoul. Moreover, observations used to Experiment A can provide appropriate assimilation results because of the wide distribution of the NIES LIDAR network.

The NIES LIDAR observation sites that are widely distributed throughout the Japanese Archipelago captured the dust event extensively, and could derive the good assimilation results. The distribution and location of observation sites strongly affect the performance of data assimilation. The planning of the new observation network can be more effective by intensive integration of observation and numerical model based on the data assimilation.

For this study, we used observation data only from the LIDAR network. However, 4D-Var can assimilate observations obtained by various platforms (e.g., surface and satellite observations) simultaneously. The assimilation of these different data will increase the performance of the assimilation. It is the next step of 4D-Var inversions for dust emissions.

Acknowledgements. This work was partly supported by the Global Environment Research Fund, Ministry of Environment, Japan and a Grant-in-Aid for Scientific Research under Grant No. 17360259 from the Ministry of Education, Culture, Sports, Science and Technology, Japan. The authors wish to acknowledge for PM₁₀ and PM_{2.5} data Japan Acid Deposition Survey (JADS) used for model validation. The CALIPSO data were obtained from the NASA Langley Research Center Atmospheric Sciences Data Center.

References

- Awaji, T., Masuda, S., Ishikawa, Y., Sugiura, N., Toyoda, T., and Nakajima, T.: State estimation of the North Pacific Ocean by a four-dimensional variational data assimilation experiment, *J. Oceanogr.*, 59, 931–943, 2003.
- Benjamin, S. G., Dévényi, D., Weygandt, S. S., et al.: An hourly assimilation-forecast cycle: The RUC, *Mon. Weather Rev.*, 132(2), 495–518, 2004.
- Carmichael, G. R., Sandu, A., Chai, T., Daescu, D. N., Constantinescu, E. M., and Tang Y.: Predicting Air Quality: Current Status and Future Directions, *J. Comput. Phys.*, in press, 2007.

Numerical modeling of Asian dust with adjoint inversion

K. Yumimoto et al.

Title Page

Abstract

Introduction

Conclusions

References

Tables

Figures

◀

▶

◀

▶

Back

Close

Full Screen / Esc

Printer-friendly Version

Interactive Discussion

Chai, T., Carmichael, G. R., Sandu, A., Tang, Y., and Daescu D. N.: Chemical data assimilation of transport and chemical evolution over the Pacific (TRACE-P) aircraft measurements, *J. Geophys. Res.*, 111, D02301, doi:10.1029/2005JD005883, 2006.

Chai, T., Carmichael, G. R., Tang, Y., et al.: Four-dimensional data assimilation experiments with International Consortium for Atmospheric Research on Transport and Transformation ozone measurement, *J. Geophys. Res.*, 112, D12S15, doi:10.1029/2006JD007763, 2007.

Draxler, R. R. and Hess, G. D.: An overview of the HYSPLIT_4 modelling system for trajectories, dispersion, and deposition, *Aust. Meteorol. Mag.*, 47, 295–308, 1998.

Elbern, H. and Schmidt, H.: A 4D-Var chemistry data assimilation scheme for Eulerian chemistry transport modeling, *J. Geophys. Res.*, 104(D15), 18 583–18 598, 1999.

Elbern, H. and Schmidt H.: Ozone episode analysis by four-dimensional variational chemistry data assimilation, *J. Geophys. Res.*, 106(D4), 3569–3590, 2001.

Elbern, H., Schmidt, H., and Ebel A.: Variational data assimilation for tropospheric chemistry modeling, *J. Geophys. Res.*, 102(D13), 15 967–15 985, 1997.

Elbern, H., Strunk, A., Schmidt, H., and Talagrand O.: Emission rate and chemical state estimation by 4-dimensional variational inversion, *Atmos. Chem. Phys.*, 7, 3749–3769, 2007, <http://www.atmos-chem-phys.net/7/3749/2007/>.

Fernald, F. G.: Analysis of atmospheric LIDAR observations: Some comments, *Appl. Opt.*, 23, 652–653, 1984.

Gong, S. L., Zhang, X. Y., Zhao, T. L., McKendry, I. G., Jaffe, D. A., and Lu, N. M.: Characterization of soil dust aerosol in China and its transport and distribution during 2001 ACE-Asia: 2. Model simulation and validation, *J. Geophys. Res.*, 108(D9), 4262, doi:10.1029/2002JD002633, 2003.

Hakami, A., Henze, D. K., Seinfeld, J. H., Chai, T., Tang, Y., Carmichael, G. R., and Sandu, A.: Adjoint inverse modeling of black carbon during the Asian Pacific Regional Aerosol Characterization Experiment, *J. Geophys. Res.*, 110, D14301, doi:10.1029/2004JD005671, 2005.

Henze, D. K., Hakami, A., and Seinfeld, J. H.: Development of the adjoint of GEOS-Chem, *Atmos. Chem. Phys.*, 7, 2431–2433, 2007, <http://www.atmos-chem-phys.net/7/2431/2007/>.

Hu, X. Q., Lu, N. M., Niu, T., and Zhang P.: Operational retrieval of Asian sand and dust storm from FY-2C geostationary meteorological satellite and its application to real time forecast in Asia, *Atmos. Chem. Phys. Discuss.*, 7, 8395–8421, 2007, <http://www.atmos-chem-phys-discuss.net/7/8395/2007/>.

Numerical modeling of Asian dust with adjoint inversion

K. Yumimoto et al.

Title Page

Abstract

Introduction

Conclusions

References

Tables

Figures

◀

▶

◀

▶

Back

Close

Full Screen / Esc

Printer-friendly Version

Interactive Discussion

- Liu, D. C. and Nocedal J.: On the limited memory BFGS method for large scale optimization, *Math. Program.*, 45, 503–528, 1989.
- Liu, Z., Sugimoto, N., and Murayama T.: Extinction-to-backscatter ratio of Asian dust observed with high-spectral-resolution LIDAR and Raman LIDAR, *Appl. Optics*, 41, 2760–2767, 2002.
- 5 Liu, Z., Vaughan, M. A., Winker, D. M., Hostetler, C. A., Poole L. R., Hlavka, D., Hart, W., and McGill, M. Use of probability distribution functions for discriminating between cloud and aerosol in lidar backscatter data, *J. Geophys. Res.*, 109, D15202, doi:10.1029/2004JD004732, 2004.
- Liu, M., Westphal, D. L., Wang, S., Shimizu, A., Sugimoto, N., Zhou, J., and Chen, Y.: A
10 high-resolution numerical study of the Asian dust storms of April 2001, *J. Geophys. Res.*, 108(D23), 8653, doi:10.1029/2002JD003178, 2003.
- Martien, P. T., Harley, R. A., and Cacuci, D. G.: Adjoint sensitivity analysis for a three-dimensional photochemical model: implementation and method comparison, *Environ. Sci. Technol.*, 40(8), 2663–2670, doi:10.1021/es0510257, 2006.
- 15 Müller, J.-F. and Stavrou, T.: Inversion of CO and NO_x emissions using the adjoint of the IMAGES model, *Atmos. Chem. Phys.*, 5, 1157–1186, 2005,
<http://www.atmos-chem-phys.net/5/1157/2005/>.
- Niu, T., Gong, S. L., Zhu, G. F., Liu, H. L., Hu, X. Q., Zhou, C. H., and Wang, Y. Q.: Data
20 assimilation of dust aerosol observations for CUACE/Dust forecasting system, *Atmos. Chem. Phys. Discuss.*, 7, 8309–8332, 2007,
<http://www.atmos-chem-phys-discuss.net/7/8309/2007/>.
- Overpeck, J., Rind, D., Lacis, A., and Healy, R.: Possible role of dust-induced regional warming in abrupt climate change during the last glacial period, *Nature*, 384, 447–449, 1996.
- Pielke, R. A., Cotton, W. R., Walko, R. L., et al.: A comprehensive meteorological modeling
25 system: RAMS, *Meteorol. Atmos. Phys.*, 49, 69–91, 1992.
- Remer, L. A., Kaufman, Y. J., Tanré, D., et al.: The MODIS Aerosol Algorithm, Products and Validation, *J. Atmos. Sci.*, 62, 947–973, 2005.
- Shao, Y., Yang, Y., Wang, J., et al.: Northeast Asian dust storms: Real-time numerical prediction and validation, *J. Geophys. Res.*, 108(D22), 4691, doi:10.1029/2003JD003667, 2003.
- 30 Shimizu, A., Sugimoto, N., Matsui, I., et al.: Continuous observations of Asian dust and other aerosols by polarization lidars in China and Japan during ACE-Asia, *J. Geophys. Res.*, 109(D19S17), doi:10.1029/2002JD003253, 2004.
- Sokolik, I. N. and Toon, O. B.: Direct radiative forcing by anthropogenic airborne mineral

**Numerical modeling
of Asian dust with
adjoint inversion**K. Yumimoto et al.

Title Page

Abstract

Introduction

Conclusions

References

Tables

Figures

◀

▶

◀

▶

Back

Close

Full Screen / Esc

Printer-friendly Version

Interactive Discussion

- aerosols, *Nature*, 381, 681–683, 1996.
- Sugimoto, N., Matsui, I., Shimizu, A., Uno, I., Arai, K., Endoh, T., and Nakajima, T.: Observation of dust and anthropogenic aerosol plumes in the Northwest Pacific with a two-wavelength polarization lidar on board the research vessel Mirai, *Geophys. Res. Lett.*, 29(19), 1901, doi:10.1029/2002GL015112, 2002.
- Sugimoto, N., Shimizu, A., Matsui, I., Dong, X., Zhou, J., Bai, X., Zhou, J., Lee, C.-H., Yoon, S.-C., Okamoto, H., and Uno, I.: Network Observations of Asian Dust and Air Pollution Aerosols Using Two-Wavelength Polarization Lidars, 23rd International Laser Radar Conference, July 2006 Nara, Japan (23ILRC, ISBN 4-9902916-0-3), 851–854, 2006.
- Stavrakou, T. and Müller, J.-F.: Grid-based versus big region approach for inverting CO emissions using Measurement of Pollution in the Troposphere (MOPITT) data, *J. Geophys. Res.*, 111, D15304, doi:10.1029/2005JD006896, 2006.
- Takemura, T., Okamura, H., Maruyama, Y., Numaguti, A., Higurashi, A., and Nakajima, T.: Global three-dimensional simulation of aerosol optimal thickness distribution of various origins, *J. Geophys. Res.*, 105(17), 853–17873, 2000.
- Tanaka, T. Y. and Chiba, M.: Global simulation of dust aerosol with a chemical transport model, MASINGAR, *J. Meteorol. Soc. Jpn.*, 83A, 255–278, 2005.
- Uno, I., Carmichael, G. R., Streets, D. G., et al.: Numerical study of Asian dust transport during the springtime of 2001 simulated with the Chemical Weather Forecasting System (CFORS) model, *J. Geophys. Res.*, 109, D19S24, doi:10.1029/2003JD00422, 2004.
- Uno, I., Harada, K., Satake, S., Hara, Y., and Wang, Z.: Meteorological Characteristics and Dust Distribution of the Tarim Basin Simulated by the RAMS/CFORS Dust Model, *J. Meteorol. Soc. Jpn.*, 83A, 219–239, 2005.
- Uno, I., Wang, Z., Chiba, M., et al.: Dust model intercomparison (DMIP) study over Asia: Overview, *J. Geophys. Res.*, 111, D12213, doi:10.1029/2005JD006575, 2006.
- Winker, D. M., Hunt, W. H., and McGill, M. J.: Initial performance assessment of CALIOP, *Geophys. Res. Lett.*, 34, L19803, doi:10.1029/2007GL030135, 2007.
- Yumimoto, K. and Uno, I.: Adjoint inverse modeling of CO emissions over the East Asian region using four dimensional variational data assimilation, *Atmos. Environ.* 40, 6836–6845, 2006.
- Yumimoto, K., Uno, I., Sugimoto, N., Shimizu, A., and Satake, S.: Adjoint inverse modeling of dust emission and transport over East Asia, *Geophys. Res. Lett.*, 34, L00806, doi:10.029/2006GL028551, 2007.

**Numerical modeling
of Asian dust with
adjoint inversion**K. Yumimoto et al.

[Title Page](#)[Abstract](#)[Introduction](#)[Conclusions](#)[References](#)[Tables](#)[Figures](#)[◀](#)[▶](#)[◀](#)[▶](#)[Back](#)[Close](#)[Full Screen / Esc](#)[Printer-friendly Version](#)[Interactive Discussion](#)

Numerical modeling of Asian dust with adjoint inversion

K. Yumimoto et al.

Table 1. Observation sites of NIES LIDAR and JADS PM measurement: RMS error and mean values at each site.

Obs	Group	site	RMSE		MEAN	
			(not assimilated / A / B)		(obs/not assimilated/A/B)	
NIES LIDAR (dust ext., 1/km) ^a	B	Beijing	(B)	0.43/0.46/0.44	0.45/0.20/0.27/0.25	
	B	Seoul	(S)	0.29/0.21/0.20	0.28/0.14/0.28/0.25	
	A, B	Matsue	(Mts)	0.29/0.18/0.20	0.27/0.089/0.19/0.17	
	A, B	Hedo-Okinawa	(H)	0.074/0.060/0.064	0.060/0.016/0.031/0.027	
	A, B	Nagasaki	(Ng)	0.13/0.13/0.13	0.13/0.071/0.13/0.12	
	A, B	Toyama	(Ty)	0.19/0.13/0.13	0.16/0.062/0.14/0.13	
	A, B	Tsukuba	(Ts)	0.071/0.10/0.093	0.095/0.061/0.12/0.10	
JADS PM (PM ₁₀ , μg/m ³)		Banryu	(Bn)	141.7/165.8/148.3	102.6/57.0/142.9/126.9	(μg/m ³)
		Sado	(Sd)	65.7/116.0/105.4	54.7/44.4/105.4/93.1	(μg/m ³)
		Hedo-Okinawa	(H)	57.0/81.8/74.9	46.8/19.0/39.4/35.4	(μg/m ³)
		Rishiri	(Rs)	36.7/40.3/38.1	17.7/14.3/23.4/19.3	(μg/m ³)

^a The RMS errors and mean values are computed based on the dust AOT calculated by integration of the dust ext. coefficient.

[Title Page](#)
[Abstract](#)
[Introduction](#)
[Conclusions](#)
[References](#)
[Tables](#)
[Figures](#)
[◀](#)
[▶](#)
[◀](#)
[▶](#)
[Back](#)
[Close](#)
[Full Screen / Esc](#)
[Printer-friendly Version](#)
[Interactive Discussion](#)

Numerical modeling of Asian dust with adjoint inversion

K. Yumimoto et al.

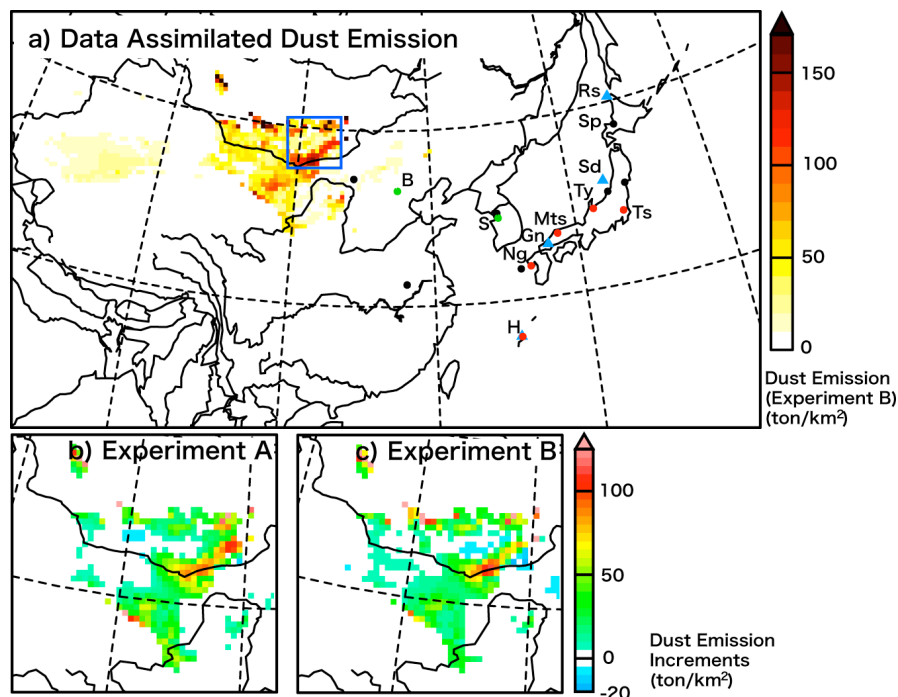


Fig. 1. Model region and NIES LIDAR observation sites. **(a)** Assimilated dust emission intensity from 20 March to 3 April (Experiment B). Circles denote NIES LIDAR observation sites: Sapporo (Sp), Tsukuba (Ts), Matsue (Mts), Nagasaki (Ng), Hedo-Okinawa (H), Seoul (S), and Beijing (B). Red circles denote observation sites used in both Experiment A and Experiment B. Green circles denote additional observation sites of Experiment B. Blue triangles denote PM observation sites. **(b)** Dust emission increment for w/o assimilation and assimilated (Experiment A). **(c)** Dust emission increment for w/o assimilation and assimilated (Experiment B).

Title Page

Abstract

Introduction

Conclusions

References

Tables

Figures

◀

▶

◀

▶

Back

Close

Full Screen / Esc

Printer-friendly Version

Interactive Discussion

**Numerical modeling
of Asian dust with
adjoint inversion**

K. Yumimoto et al.

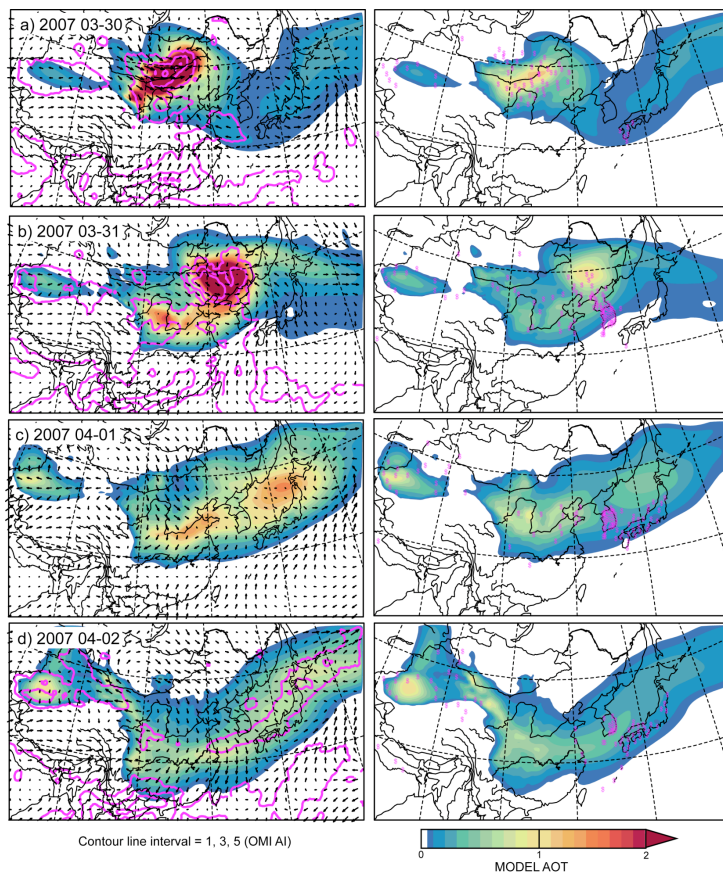


Fig. 2. Comparison of horizontal distributions of modeled AOT and OMI AI: the left column shows assimilated AOT (color) and OMI AI (pink lines; interval = 1, 3, 5); the right column shows model dust AOT without assimilation (color) and SYNOP dust report (pink \$ symbols).

Title Page

Abstract

Introduction

Conclusions

References

Tables

Figures

◀

▶

◀

▶

Back

Close

Full Screen / Esc

Printer-friendly Version

Interactive Discussion

Numerical modeling
of Asian dust with
adjoint inversion

K. Yumimoto et al.

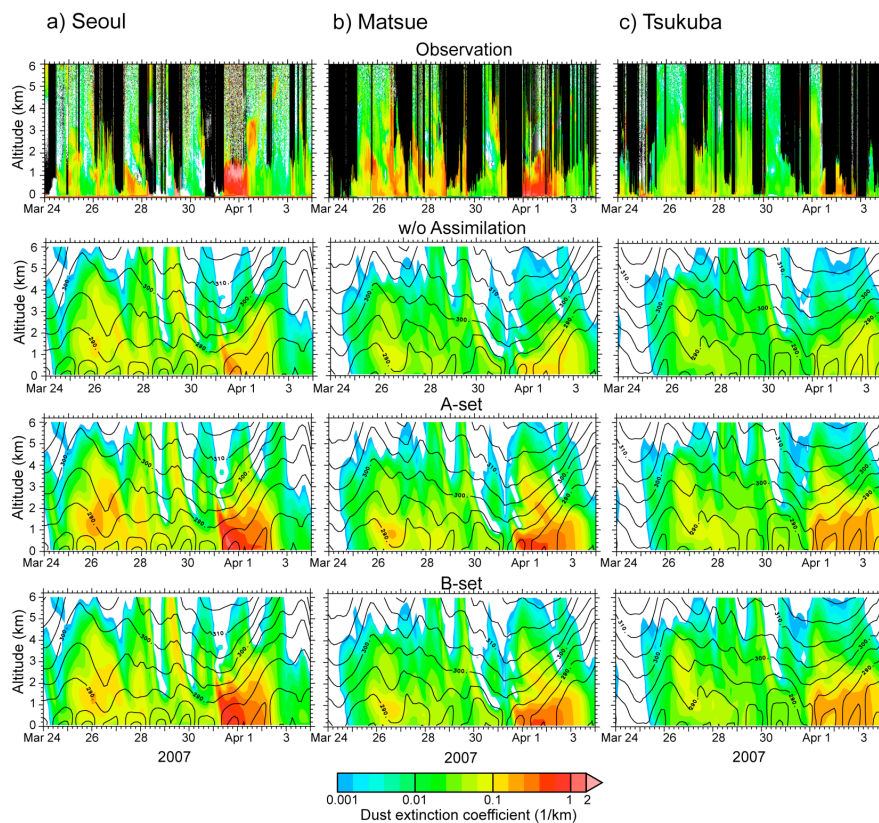


Fig. 3. Time-Height plots of dust extinction coefficients (log-scaled) at Seoul, Matsue, and Tsukuba. The first row shows NIES LIDAR observation. Second, third, and fourth rows respectively show modeled dust extinction for w/o assimilation, assimilated (Experiment A) and assimilated (Experiment B).

[Title Page](#)[Abstract](#)[Introduction](#)[Conclusions](#)[References](#)[Tables](#)[Figures](#)[◀](#)[▶](#)[◀](#)[▶](#)[Back](#)[Close](#)[Full Screen / Esc](#)[Printer-friendly Version](#)[Interactive Discussion](#)

Numerical modeling of Asian dust with adjoint inversion

K. Yumimoto et al.

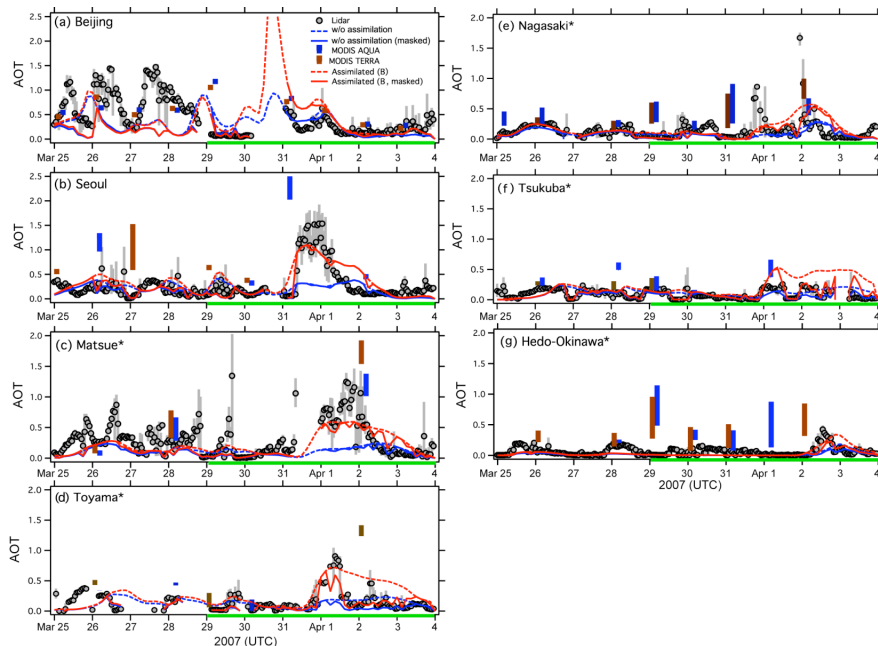


Fig. 4. Time series of LIDAR and modeled, MODIS AOT at NIES LIDAR sites. Circles denote the 1-h-average of dust AOT calculated using LIDAR observations. Gray bars denote ranges between minimum and maximum of LIDAR dust AOT. Red lines show assimilated dust AOTs; blue lines are those without assimilation. Solid lines denote model dust AOTs, which take missing LIDAR points into account. Blue and orange box bars denote total AOT (box top) and coarse mode AOT (box bottom), as measured by MODIS. Observation data measured from 29 March to 4 April are assimilated (shown by green horizontal lines).

Title Page

Abstract

Introduction

Conclusions

References

Tables

Figures

◀

▶

◀

▶

Back

Close

Full Screen / Esc

Printer-friendly Version

Interactive Discussion

Numerical modeling
of Asian dust with
adjoint inversion

K. Yumimoto et al.

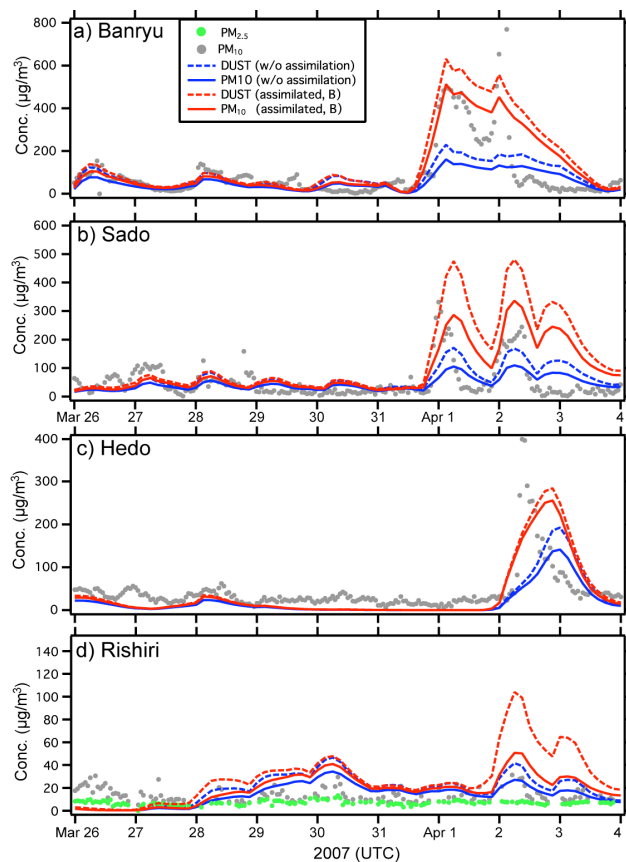


Fig. 5. Comparison of modeled (without assimilation and assimilated) and observed surface PM_{10} concentrations at Rishiri, Banryu, Sado, and Hedo-Okinawa. Circles show hourly PM_{10} and $\text{PM}_{2.5}$ (at Rishiri only) observations. Dashed lines denote modeled dust concentrations; solid lines show modeled dust PM_{10} concentrations calculated with eight smaller bins.

[Title Page](#)[Abstract](#)[Introduction](#)[Conclusions](#)[References](#)[Tables](#)[Figures](#)[◀](#)[▶](#)[◀](#)[▶](#)[Back](#)[Close](#)[Full Screen / Esc](#)[Printer-friendly Version](#)[Interactive Discussion](#)

Numerical modeling of Asian dust with adjoint inversion

K. Yumimoto et al.

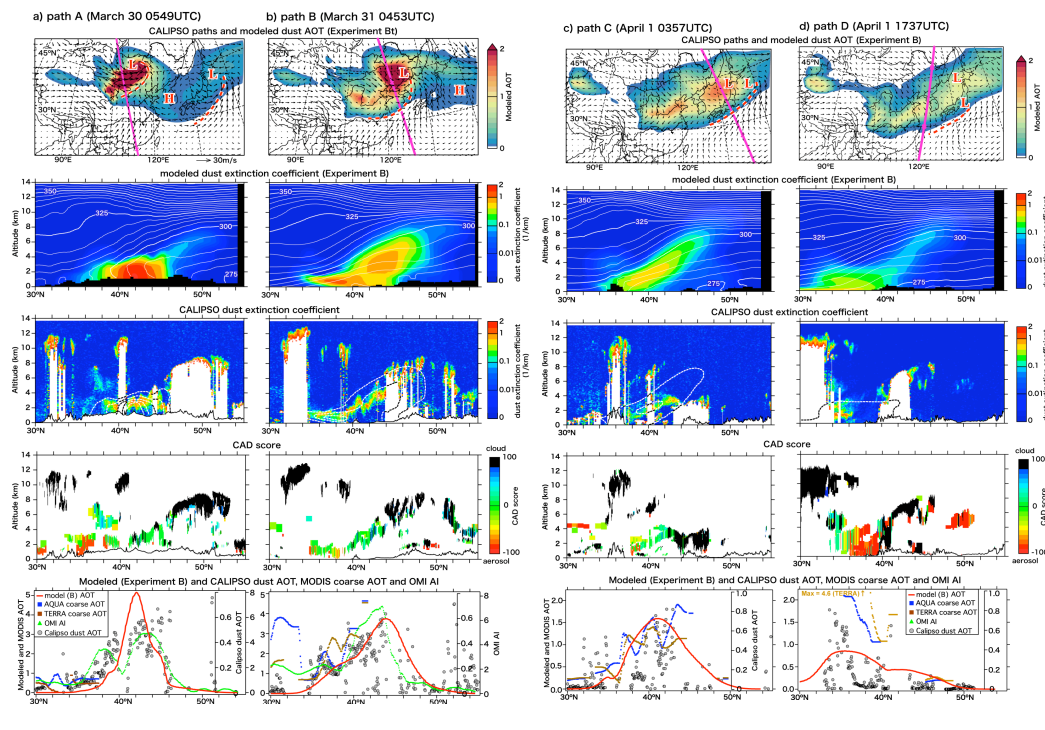


Fig. 6. Comparison of modeled and CALIPSO dust extinction coefficients. The first row shows CALIPSO observation paths and modeled dust AOT (Experiment B) and surface winds. L is the low-pressure; red broken lines denote its cold front. The second row shows modeled dust extinction coefficients (color) and potential temperature (white line) along the CALIPSO observation path. The third row shows the CALIPSO dust extinction coefficient (color); broken lines denote the modeled dust extinction coefficient ($0.5, 1.0, 1.5, 2 \text{ km}^{-1}$). The fourth row shows the CAD score. The fifth row shows the modeled dust AOT (left axis), CALIPSO dust AOT (right inside axis), MODIS coarse AOT (left axis), and OMI AI (right axis) along the CALIPSO path.

[Title Page](#)
[Abstract](#)
[Introduction](#)
[Conclusions](#)
[References](#)
[Tables](#)
[Figures](#)
[◀](#)
[▶](#)
[◀](#)
[▶](#)
[Back](#)
[Close](#)
[Full Screen / Esc](#)
[Printer-friendly Version](#)
[Interactive Discussion](#)

Numerical modeling
of Asian dust with
adjoint inversion

K. Yumimoto et al.

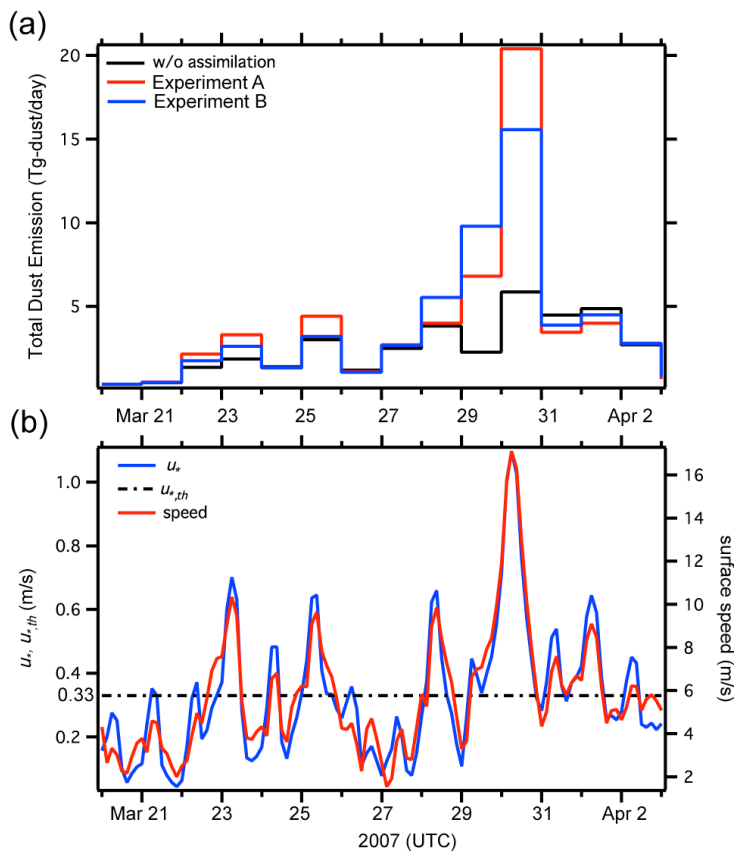


Fig. 7. Daily dust emission flux and regional averaged surface speed and u_* , and $u_{*,th}$ through-out the region depicted in Fig. 1a.

[Title Page](#)[Abstract](#)[Introduction](#)[Conclusions](#)[References](#)[Tables](#)[Figures](#)[◀](#)[▶](#)[◀](#)[▶](#)[Back](#)[Close](#)[Full Screen / Esc](#)[Printer-friendly Version](#)[Interactive Discussion](#)